Artificial Photosynthesis of C1–C3 Hydrocarbons from Water and CO 2 on Titanate Nanotubes Decorated with Nanoparticle Elemental Copper and CdS Quantum Dots

ARTICLE *in* THE JOURNAL OF PHYSICAL CHEMISTRY A · JANUARY 2015

Impact Factor: 2.69 · DOI: 10.1021/jp511329d · Source: PubMed

4 AUTHORS, INCLUDING:

Agustin J Colussi
California Institute of Technology
214 PUBLICATIONS **4,229** CITATIONS
SEE PROFILE

Michael R. Hoffmann
California Institute of Technology
379 PUBLICATIONS **30,187** CITATIONS
SEE PROFILE

THE JOURNAL OF PHYSICAL CHEMISTRY A

Article

pubs.acs.org/JPCA

Artificial Photosynthesis of C1−C3 Hydrocarbons from Water and CO_2 on Titanate Nanotubes Decorated with Nanoparticle Elemental Copper and CdS Quantum Dots

Hyunwoong Park,[†] Hsin-Hung Ou,[‡] Agustín J. Colussi,[‡] and Michael R. Hoffmann*[,‡]

[†]School of Energy Engineering, Kyungpook National University, Daegu 702-701, Korea

[‡]Linde+Robinson Laboratory, California Institute of Technology, Pasadena, California 91125, United States

Supporting Information

ABSTRACT: The conversion of CO_2 and water into value-added fuels with visible light is difficult to achieve in inorganic photocatalytic systems. However, we synthesized a ternary catalyst, CdS/(Cu-TNTs), which is assembled on a core of sodium trititanate nanotubes (TNTs; $Na_xH_{2-x}Ti_3O_7$) decorated with elemental copper deposits followed by an overcoat of CdS quantum dot deposits. This ternary photocatalyst is capable of catalyzing the conversion of CO_2 and water into C1−C3 hydrocarbons (e.g., CH_4, C_2H_6, C_3H_8, C_2H_4, C_3H_6) upon irradiation with visible light above 420 nm. With this composite photocatalyst, sacrificial electron donors are not required for the photoreduction of CO_2. We have shown that water is the principal photoexcited-state electron donor, while CO_2 bound to the composite surface serves as the corresponding electron acceptor. If the photochemical reaction is carried out under an atmosphere of 99.9% $^{13}CO_2$, then the product hydrocarbons are built upon a ^{13}C backbone. However, free molecular H_2 is not observed over 5 h of visible light irradiation even though proton reduction in aqueous solution is thermodynamically favored over CO_2 reduction. In terms of photocatalytic efficiency, the stoichiometric fraction of Na^+ in TNTs appears to be an important factor that influences the formation of the observed hydrocarbons. The coordination of CO_2 to surface exchange sites on the ternary catalyst leads to the formation of surface-bound CO_2 and related carbonate species. It appears that the bidentate binding of O═C═O to certain reactive surface sites reduces the energy barrier for conduction band electron transfer to CO_2. The methyl radical ($CH_3^•$), an observed intermediate in the reaction, was positively identified using an ESR spin trapping probe molecule. The copper deposits on the surface of TNTs appear to play a major role in the transient trapping of methyl radical, which in turn self-reacts to produce ethane.

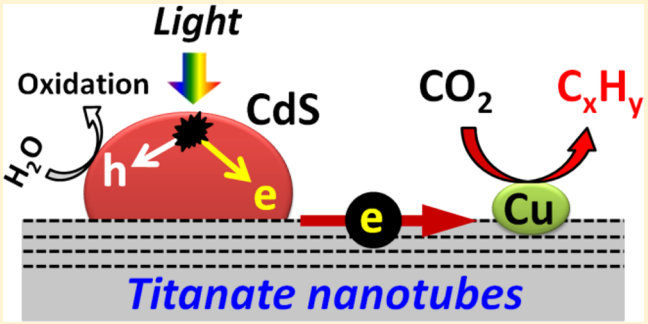

INTRODUCTION

Many technical solutions have been explored to reduce CO_2 emissions to the atmosphere. These include carbon sequestration in the subsurface terrestrial or marine environments and sorption and trapping in appropriate solvents or within macroporous, multifunctional materials. Along with physical sequestration and long-term storage, there is renewed interest in the catalytic photoreduction of CO_2 to form useful hydrocarbons.[1−9] In order to promote CO_2 reduction, a large potential energy barrier must be overcome to achieve the initial one-electron reduction of CO_2.[10−13] For example, the reduction potential for the one-electron reduction of CO_2 to form the carbon dioxide radical anion ($CO_2^{•−}$) is −1.97 V.[1]

In previous work, C1 reduction products such as CO,[7,9] HCOOH,[10,14−17] CH_3OH,[18] and CH_4[2] were reported using illuminated semiconductor catalysts. Photocatalytic formation of C2 compounds (e.g., C_2H_6 and C_2H_4) has also been reported.[8,19] On the other hand, sacrificial electron donors are often required to achieve measurable product yields.[14,15,17,20] As a consequence, a large uncertainty in the CO_2 reduction pathways and actual CO_2-derived product yields are introduced due to the use of organic compounds as sacrificial reagents.[6] In order to resolve this uncertainty, high-purity $^{13}CO_2$ can be used as an isotopic tracer to track the contributions from residual organic reagents or solvents (e.g., isopropanol) to the observed product distributions and yields. Most often, sacrificial reagents such as oxalate and aliphatic alcohols are used as electron donors in order to enhance overall reaction kinetics and apparent quantum yields and to increase the product yields.[6] For example, Yang et al. showed that carbon-containing residues remaining from catalyst syntheses can contribute to the array of observed carbon-containing reaction products during photocatalytic CO_2 reduction.[7] Under ideal conditions,

Special Issue: Mario Molina Festschrift

Received: November 12, 2014
Revised: January 21, 2015
Published: January 22, 2015

DOI: 10.1021/jp511329d
J. Phys. Chem. A 2015, 119, 4658−4666

a suitable photocatalyst for artificial photosynthesis should be made from earth-abundant materials that are activated by visible light above 420 nm and use water as the sole source of electrons for the conversion of CO_2 into value-added hydrocarbon products.

The conversion of CO_2 into C1−C3 hydrocarbons using only water, CO_2, and visible light in the presence of suitable semiconductor catalysts without added sacrificial electron donors remains a challenge.[9,19,21] In our experiments, a composite, hybrid catalyst has a base of sodium trititanate ($Na_xH_{2-x}Ti_3O_7$) nanotubes decorated with surface deposits of elemental copper (Cu^0) and sequential deposits of CdS quantum dots to produce a ternary photocatalyst. Variations in the stoichiometric level, x, were probed during catalyst preparation in order to investigate the effect of an alkali promoter such as Na^+ on the CO_2 photoreduction.

EXPERIMENTAL SECTION

Preparation of Catalysts. Trititanate nanotubes (TNTs; $Na_xH_{2-x}Ti_3O_7$) were synthesized by a modified hydrothermal method.[22−24] In a typical preparation process, 0.7 g of TiO_2 was stirred in aqueous NaOH solution (10 M, 35 mL) for 30 min in a Teflon-lined container (50 mL). The container was subsequently put into a stainless steel autoclave and then transferred to an electronic oven at around 130 °C for 24 h. After hydrothermal treatment, the resulting powders were rinsed with different volumes (10, 20, and 30 mL) of 6 M HCl to obtain three levels of sodium amounts within TNTs. The Na/Ti ratios determined by energy-dispersive X-ray spectrometry were 0.093, 0.143, and 0.507 for $Na_xH_{2-x}Ti_3O_7$, which we classify for simplicity as low, medium, or high values of x, respectively. Around 50 mL of deionized water was used to wash off the excess sodium and chloride ions adhered on the catalyst surface. TNT powders were obtained after centrifugation (Marathon 22k, Fisher Scientific) and drying (Freezone 4.5 LABCONCO). For copper-modified TNTs, 2% of Cu(II) ($Cu(NO_3)_2$) relative to the amount of TNTs by weight was mixed in a 20 mL of deionized water for 3 h. The slurry was then centrifuged and dried to obtain Cu^{2+}-TNTs. The sample powders were subsequently baked at 350 °C in a tubular furnace in a 20% H_2/80% N_2 (v/v) atmosphere to obtain Cu/TNTs. For coupling with CdS, 0.5 g of the resulting powders (bare TNTs and Cu^{2+}-TNTs) were stirred in aqueous cadmium acetate ($Cd(CH_3COO)_2{\cdot}2H_2O$) solution (20 mM, 30 mL) for 3 h, followed by sulfurization with $Na_2S{\cdot}9H_2O$ (20 mM) in the aforementioned Teflon-lined autoclave at 180 °C for 24 h.[25] The resulting samples were washed with deionized water several times and subjected to the centrifugation and drying. They were subsequently baked at 350 °C in a tubular furnace in a 20% H_2/80% N_2 (v/v) atmosphere to obtain CdS-TNTs and CdS/(Cu-TNTs). For comparison, Cu was incorporated into the presynthesized CdS-TNTs (i.e., Cu/(CdS-TNTs) by following the same procedure.

Characterizations of the Catalyst. Sample powders were ground with a pestle in a mortar and pressed using a pelletizer to obtain thin disks. Then, the crystal structure of the sample was identified by X-ray diffraction using a Philips diffractometer (X'pert Pro) with Cu Kα radiation. UV−vis diffuse reflectance spectra of catalysts were obtained using a spectrophotometer (Shimadzu UV-2101PC). For this, sample powders were mixed with $BaSO_4$, and their absorption spectra were measured with respect to $BaSO_4$.[26] Diffuse reflectance infrared Fourier transform (DRIFT) spectra of catalysts were acquired with a Nicolet 6700 FTIR spectrometer attached with a liquid-N_2-cooled MCT detector at a 8 cm^{-1} resolution using a Spectra-Tech Controller diffuse reflectance accessory. For DRIFT analysis, a catalyst slurry (50 mg of target catalyst in 25 mL of deionized water) was prepared, and then, the suspension was purged with CO_2 for 30 min in the dark. The resulting slurry was then centrifuged at 8000 rpm for 1 min, and then, the centrifuged powder was isolated after freeze-drying for 20 h (−45 °C; 80−100 mTorr). X-ray photoelectron spectroscopy (XPS) data were obtained at a base pressure of $<1 \times 10^{-9}$ Torr using an M-probe spectrometer. High-resolution spectra were controlled using the ESCA 2000E Capture software (Service Physics). All spectra were calibrated by the binding energy of C 1s at 284.6 eV. Specific surface areas and Na/Ti ratios of the prepared samples were also determined with a Micromeritics ASAP 2010 surface area analyzer and energy dispersive X-ray spectroscopy (JEOL JSM-6500F), respectively

CO_2 Photocatalysis and Product Analysis. In a typical experiment, 50 mg of the prepared catalyst was suspended in 25 mL of deionized water in an airtight glass reactor (~33 mL) with a quartz window. The reactor was sealed tightly with a rubber stopper and then purged with CO_2 for 1 h, and illumination started using a 450 W Xe lamp in combination with a 420 nm cutoff filter. The reaction temperature was controlled in the range of 20−25 °C.

The gas composition in the headspace was analyzed periodically by gas chromatography (HP 6890 Series II) coupled with a mass-selective detector (HP 5972 Series II). This device was equipped with an HP-5ms capillary column, a split/split-less injector with a Merlin microseal high-pressure septum, and an insert liner of 0.75 mm i.d. The electron ionization energy was set at 70 eV, and the selected-ion monitoring (SIM) mode was used for the quantitative measurements. The mass spectral ions (m/z) used for quantification were 16 for CH_4, 26 for C_2H_4/C_2H_6, 41 for C_3H_6/C_3H_8, and 43 for C_4H_{10}. For quantification of identified hydrocarbons, a mixed standard hydrocarbon gas (methane, ethane, propane, ethylene, propylene, etc.; each 15 ppm, Supelco) with helium carrier gas at 8.6 $mL{\cdot}min^{-1}$ was flowed through an HP-Plot Q column (0.53 mm ID) equipped in a gas chromatography (HP 5890 Series II) with a flame ionization detector (detection limit of hydrocarbons ≈ 1 ppm), and standard curve fits between each standard gas concentration and corresponding spectral area were obtained. The retention times of hydrocarbons were almost invariant (e.g., methane, ethane, and propane at around 1, 2, and 4 min, respectively). GC with a thermal conductivity detector and quadrupole mass spectrometry (Balzers QMA 200) were employed for the measurements of carbon monoxide (detection limit ≈ 10^{-7} $mol{\cdot}L^{-1}$) and hydrogen gas (detection limit ≈ 5×10^{-7} $mol{\cdot}L^{-1}$), respectively.

In ^{13}C-labeled isotope experiments, the composition of the headspace gas was analyzed using GC/electron impact time-of-flight mass spectrometry (GC/EI/TOF/MS, Waters, GCT, Premier). This instrument was outfitted with a standard 6890N Agilent GC for injection of samples. Data were acquired and analyzed using MassLynx software version 4.1. The abundances of diagnostic ions were determined from the peak areas of integrated selected ion chromatograms. Isotopic $^{13}CO_2$ with a purity level of 99.9% was purchased from Cambridge Isotope Laboratories. In order to remove any contaminant ^{13}C hydrocarbons in the $^{13}CO_2$ cylinder, two hydrocarbon gas trappers (HC 2-2446 and SUPELPURE) were added in series

DOI: 10.1021/jp511329d
J. Phys. Chem. A 2015, 119, 4658−4666

to the $^{13}CO_2$ gas cylinder outflow before introducing $^{13}CO_2$ into the reaction slurry. Even with a pretrapping purification of the $^{13}CO_2$ reagent gas, a residual amount of CH_4 (~6.5 μL) was found (84.3% $^{13}CH_4$ and 15.7% $^{12}CH_4$) in the headspace of the reactor before the start of the photocatalytic reaction. However, the higher ^{13}C-containing hydrocarbons were obtained only as a result of irradiation with visible light. For example, analysis of the $^{13}CH_4$ after 7 h of reaction showed that of the total methane, 42.9% was determined to be $^{12}CH_4$, while 57.1% of the total methane, 12.7 μL, was found to be $^{13}CH_4$. During the course of the reaction, there was a 4.3-fold increase in $^{12}CH_4$ while $^{13}CH_4$ increased by only 1.3-fold.

The formation of possible radicals at initial stages (~3 min) was monitored by detecting its adduct with 5,5-dimethyl-1-pyrroline *N*-oxide (DMPO) via an electron paramagnetic resonance (EPR) spectrometer (Bruker EMX spectrometer, Bruker biospin GMBH). Before irradiation, CO_2 was purged for 10 min into the reaction slurry containing 50 mM DMPO and 50 mg of catalysts (CdS-TNTs and CdS/(Cu-TNTs)). Sample solution aliquots were obtained using 0.2 μm Nylon filters. No signals were observed for DMPO only. The specific conditions used during the EPR measurement were as follows; power = 6.44 mW; modulation amplitude, 2.00 G; and light source, 200 W xenon light equipped with a 420 nm UV cutoff filter.

RESULTS

Characterization. As shown in Figure 1a, the prepared catalyst mainly consisted of hexagonal CdS (e.g., 100, 002, 101, 110, 103, and 112 phases at 2θ = 25.57, 26.72, 27.77, 44.13, 47.89, and 52.24°, respectively; JCPDS card no. 77-2306)[27] along with trititanate and sodium titania. Furthermore, there were no discrete peaks corresponding to the Cu complex in the XRD patterns. This phenomenon can presumably be ascribed to the combinations of intercalation of Cu into TNTs and uniform distribution on the catalyst surface. No changes in the peak position and shape were found as a result of the presence of Cu, which implies that Cu does not involve the crystalline growth of CdS during thermal hydrogenation. The XRD patterns as a function of Na level within TNTs are present in Figure 1b. There was no significant difference on the XRD patterns of samples in terms of the effect of intercalated Na within TNTs. The peak intensity of sodium titania increased with increasing Na level, while the crystallinity of CdS appeared to be maintained at Na/Ti ≥ ~0.14 (medium level).

The diffuse reflectance UV−vis absorbance spectra of the prepared samples are shown in Figure 2. The spectra of the ternary catalyst were characterized by absorption in both the UV and the visible with band edges over a range between 570 and 620 nm. An increase in the intercalated Na amount within TNTs led to a significant background in the visible region. The effective band gap of the ternary catalyst was estimated at 2.25 eV by linear extrapolation from the inflection point of the curve to the baseline. The XPS spectra of CdS/(Cu-TNTs) showed a characteristic peak at 535.3 eV that can be attributed to the Na KL_1L_{23} Auger transition[28] (Figures S1a in the Supporting Information). This transition was not observed at the sample with the low Na amount, while the Na 1s peak intensities of the samples with the medium and high Na amounts were similar (Figure S1b, Supporting Information).

Photocatalysis. The photocatalytic reduction of CO_2 under visible light irradiation in a suspension of CdS/(Cu-TNTs) yielded primarily C1−C3 hydrocarbons that include CH_4, C_2H_6, and C_3H_8 along with smaller amounts of C_2H_4 and C_3H_6, as shown in Figure 3a. On the other hand, H_2 was not detected by headspace online mass spectrometry for which the detection limits were 0.1 μL by volume of gaseous product (~5 × 10^{-7} mol·L^{-1}) (Figure 3b). In addition, no CO was detected via GC/TCD analysis. The absence of these gases in the reactor

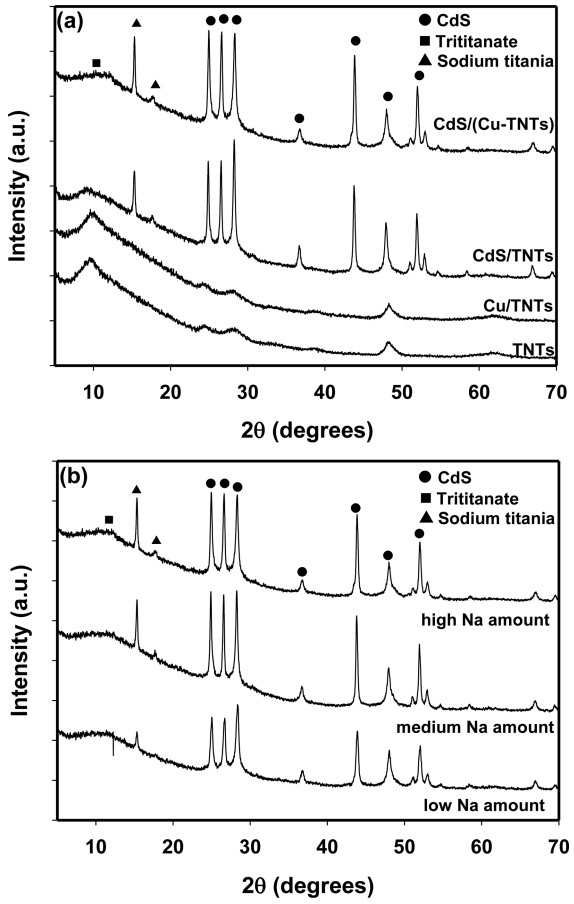

Figure 1. XRD patterns of (a) sample catalysts and (b) CdS/(Cu-TNTs) in terms of the intercalated amount of Na within TNTs. The Na/Ti ratios were 0.093 (low), 0.143 (medium), and 0.507 (high).

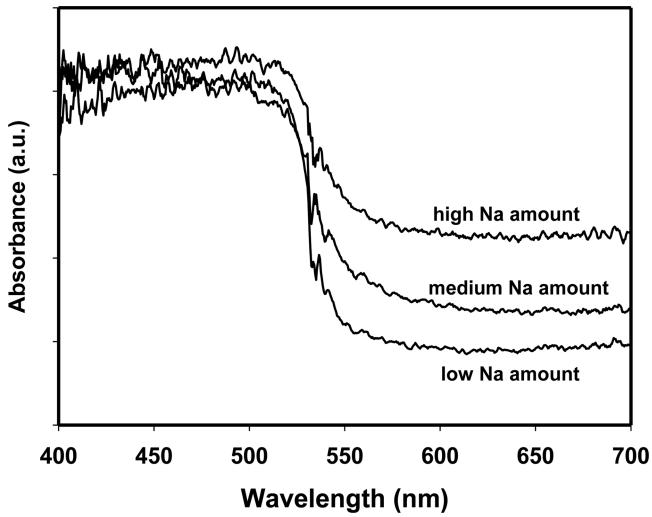

Figure 2. UV−vis diffuse reflectance spectra of CdS/(Cu-TNTs) in terms of the intercalated amount of Na within TNTs. The Na/Ti ratios were 0.093 (low), 0.143 (medium), and 0.507 (high).

DOI: 10.1021/jp511329d
J. Phys. Chem. A 2015, 119, 4658−4666

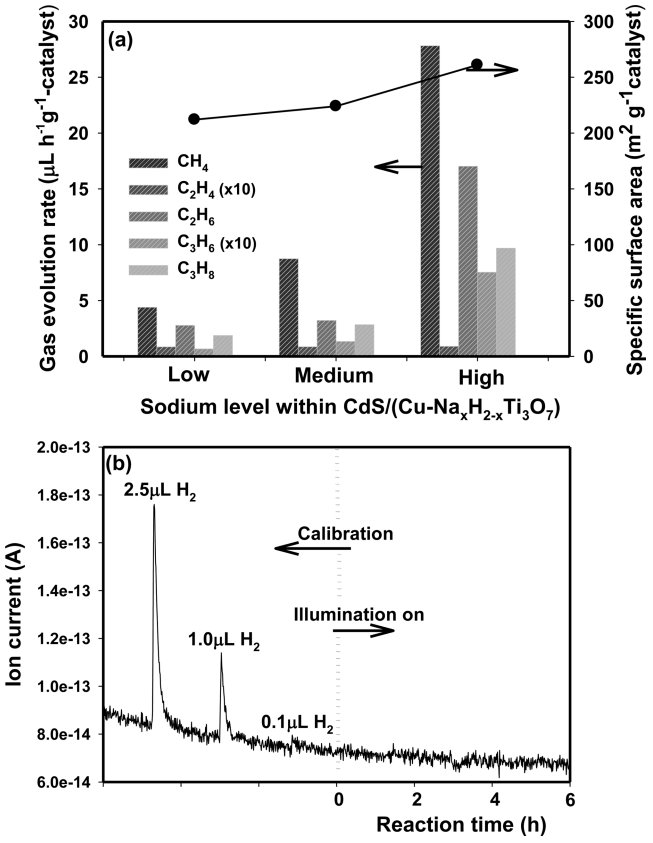

Figure 3. (a) Gas evolution rates of C1−C3 hydrocarbons on CdS/(Cu-TNTs) as a function of the intercalated Na^+ amount within TNTs (i.e., $Na_xH_{2-x}Ti_3O_7$) as well as the specific surface area. The Na/Ti ratios were 0.093 (low), 0.143 (medium), and 0.507 (high). The gas evolution rate was calculated for 5 h using 50 mg of catalyst under visible light (λ > 420 nm). (b) Quadrupole mass spectral results for determination of the detection limit for H_2 in addition to the apparent absence of detectable H_2 during 5 h of continuous irradiation of CdS/(Cu-TNTs).

headspace suggests that CO and H_2 may have been converted via a photocatalyzed Fischer−Tropsch reaction into the observable C1−C3 reaction products (R12 and R13 in Scheme 1).[1,7,29] However, successive electron transfers to CO_2 followed by protonation could also lead to the observed hydrocarbons.[30] This later possibility could be considered to be a breakthrough in photocatalytic CO_2 reduction on semiconductor surfaces in that electron transfer directly to CO_2 is apparently able to compete with electron transfer to either absorbed water or interfacial protons. This possibility is intriguing in that H_2 formation should be thermodynamically favored over CO_2 reduction in water. This implies that the self-reaction of two hydrogen atoms (R10) on the surface of CdS/(Cu-TNTs) is less probable than an encounter of a hydrogen atom and a carbon dioxide radical anion, $CO_2^{\bullet-}$ (R4).

As shown in Figure 3a, the formation rates of the C1−C3 hydrocarbons depended on the intercalated level of Na^+ within a titanium nanotube framework as well as the specific surface area. The hydrocarbon formation rates depend more on the structural modifications introduction by increasing the value of "*x*" in $Na_xH_{2-x}Ti_3O_7$ than the specific surface area of the catalyst. For example, the evolution rate of CH_4 increased by a factor of 6.5, which correlates with the 5.5-fold increase in the value of "*x*" in $Na_xH_{2-x}Ti_3O_7$ than the measured 1.3-fold increase in surface area with increasing "*x*". Nevertheless, the conversion of CO_2 to major hydrocarbons was as low as ∼0.2% primarily due to the absence of efficient electron donors and the sluggish hole transfer to water. Accordingly, the rate of production and overall yields of the C1−C3 hydrocarbons increased in the presence of the supplemental electron donors (isopropanol and formate; see Figure S2, Supporting Information). Furthermore, the yields of the olefins, C_2H_4 and C_3H_6, increased measurably.

$^{13}CO_2$ Conversion. In order to confirm that the observed hydrocarbons were actually generated via the catalytic photoreduction of CO_2, we utilized high-purity $^{13}CO_2$ as a tracer for the source of carbon (i.e., ^{13}CH versus ^{12}CH) in the measured product distribution. There has been some concern in the past that observed hydrocarbon products actually arise from trace organic contaminants present in the reaction mixture during photolysis.[7] These organic compounds may be present due to air−water scavenging of organics in the laboratory air or due to various organic compounds used as preparatory reagents (e.g., present in the $^{12}CO_2$ source gas) or solvents during synthesis, leading to uncertainty and an overestimation of relative product yields.[6,7] Results from the $^{13}CO_2$ isotopic-labeling experiments clearly show that the ^{13}C-labeled CO_2 led to the formation of an array of ^{13}C hydrocarbons even though ^{12}C hydrocarbons were also found in the product mixtures (Figure 4; see Figure

Scheme 1. Proposed Elementary Reaction Pathways of Photocatalytic CO_2 Conversion into Hydrocarbons[a]

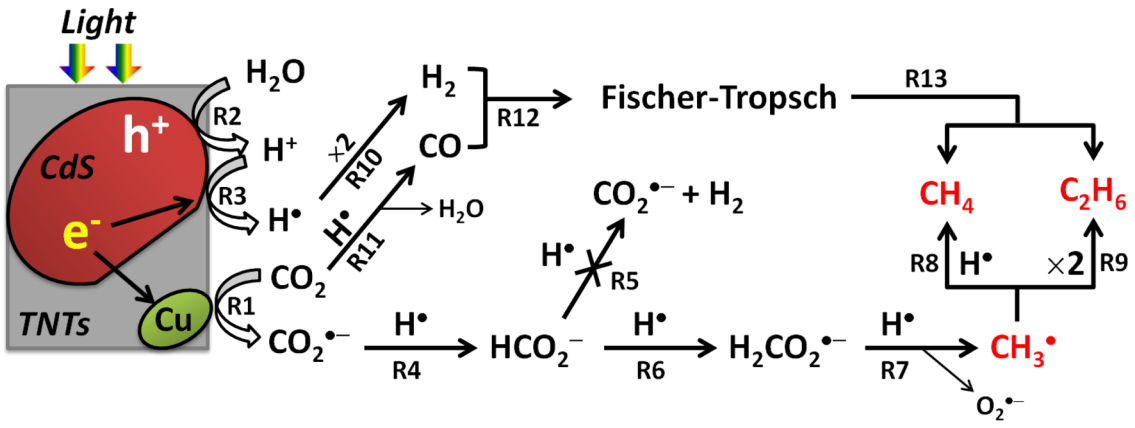

[a]Red-colored chemicals were identified in this study.

DOI: 10.1021/jp511329d
J. Phys. Chem. A 2015, 119, 4658−4666

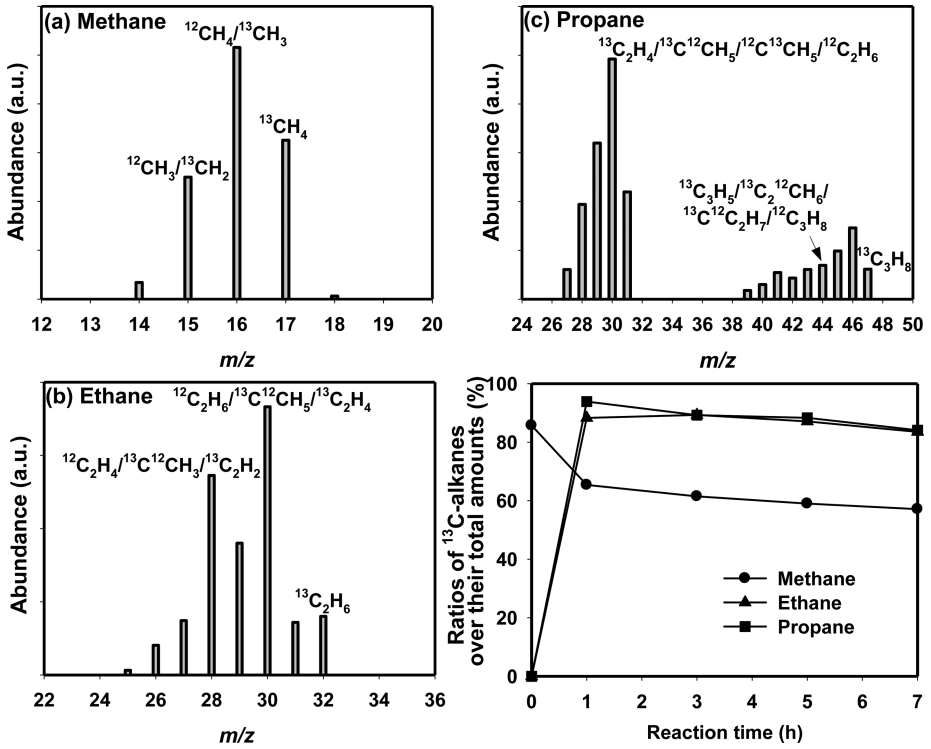

Figure 4. (a–c) Mass spectra of the observed hydrocarbons (a: methane, b: ethane, and c: propane) and (d) time profile ratios of the observed ^{13}C alkanes produced during $^{13}CO_2$ photoreduction on CdS/(Cu-TNTs) with a high level of intercalated Na^+ (Na/Ti = 0.507). The experimental conditions were the same when using $^{12}CO_2$. The mass spectra of (a) $^{13}CH_4$, (b) $^{13}C_2H_6$, and (c) $^{13}C_3H_8$ were demonstrated by taking a headspace sample after 7 h of reaction. The spectra of $^{13}C_2H_4$ and $^{13}C_3H_6$ are not shown due to signal-to-noise ratios that were considered too small to be analyzed reliably.

S3 (Supporting Information) for $^{13}CH_4$). For example, after photoreduction for 7 h, the fraction of $^{12}CH_4$ rose to 43% of the total CH_4 based on the mass spectrometric analysis of the mass-to-charge ratio at m/z = 16. Analysis of the m/z = 30 and 44 peaks for $^{13}C_2H_6$ (Figure 4b) and $^{13}C_3H_8$ (Figure 4c) shows that the ^{13}C products accounted for around 89.7 and 81.0% of the total amount, respectively, whereas the ratios of signal-to-noise for $^{13}C_2H_4$ and $^{13}C_3H_6$ of the least intense diagnostic ions were smaller than 3:1. These results indicate that various sources of ^{12}C organic compound contamination from carbon residues remaining after catalyst synthesis or introduced in the commercially produced reagents are also sources for the observed products. Figure 4d shows the time profile ratios of ^{13}C alkane yields over their respective total yields (e.g., the sum of the yields of the ^{12}C alkanes and ^{13}C alkanes). The ratios of $^{13}C_2H_6$ and $^{13}C_3H_8$ remained at around 85–90% throughout the reaction, whereas that of $^{13}CH_4$ went down to 58% after 7 h of photolysis. The relatively high level of $^{12}CH_4$ produced during prolonged photolysis suggests that either ^{12}C organic contaminants or $^{12}CO_2$ were introduced into the reaction system at some point in time. For example, if methanol, CH_3OH, residuals were present initially, the CH_4 could form via photoreduction. An alternative pathway involves a valence band hole (h^+) or trapped hole oxidation of CH_3OH to produce $^{12}CO_2$,[31−33] which is subsequently reduced by conduction band electrons mediated by the elemental copper deposits. Nonetheless, the formation of significant, measurable amounts of the ^{13}C hydrocarbons provides strong evidence for the potential of artificial photosynthesis due to the absorption of visible light by suitable ternary inorganic catalysts for the conversion of CO_2 into value-added hydrocarbon products.

DISCUSSION

Surface Complexation of CO_2. CO_2 photoreduction most likely involves the formation of the carbon dioxide radical anion ($CO_2^{\bullet-}$) that may arise from conduction band electron transfer (R1 in Scheme 1) to surface-bound carbonate species (e.g., $CO_2{\cdot}H_2O$, HCO_3^-, or CO_3^{2-}). Evidence for the surface complexation of carbonate species was presented in Figure 5, which shows the DRIFT spectra of CdS/(Cu-TNTs) exposed to CO_2 in aqueous solution in the absence of visible light. The vibrational bands in the region of 1300–1700 cm^{-1} were assigned to surface-bound carbonate species including the (bi)carbonate ions bound as a monodentate surface complex

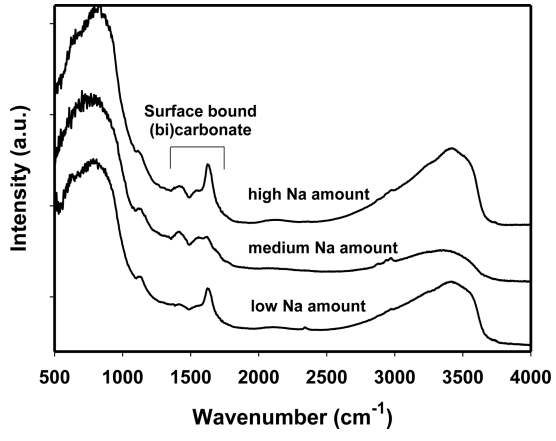

Figure 5. DRIFT spectra of CO_2-loaded catalysts as a function of the intercalated Na^+ level, x, within $Na_xH_{2-x}Ti_3O_7$.

DOI: 10.1021/jp511329d
J. Phys. Chem. A 2015, 119, 4658–4666

and/or the carbonate ions bound as a bidentate surface complex.[7,34] The strength of these vibrational bands appears to be dependent on the intercalated Na^+ fraction in $Na_xH_{2-x}Ti_3O_7$. This observation is consistent with the known effects of alkali metal promoters in CO_2 hydrogenation to produce methane.[6] The intercalated Na ions within TNTs can be distributed rather nonuniformly depending on the surface states and the preparation procedure of the catalysts. This can result in a decrease in the strength of the vibrational bands (e.g., 1625 cm^{-1}) even when the intercalated Na level increases.

Fujiwara et al. interpreted their results for CO_2 photoreduction on CdS in anhydrous DMF (i.e., no CO_2 hydration to yield HCO_3^-) using a computational model (DFT) for a CdS cluster interacting with a liner O═C═O molecule.[3] The lowest predicted energy configuration involved the bidenate complexation of CO_2 in which the bond lengths and resulting bond angle of O−C−O were found to be nearly identical to those in $CO_2^{\bullet-}$. Computational results coupled with their experimental observations led to the hypothesis that the bidentate binding of O═C═O facilitates multiple electron transfers due to longer interfacial residence. Electron transfer from the conduction band of the catalyst to hydrated CO_2 has also been reported to require the presence of suitable unoccupied molecular orbitals (i.e., LUMO states) on CO_2.[4] Because the LUMO energy decreases with decreasing O−C−O bond angle, bidentate binding of CO_2 with its reduced bond angle should be able to promote electron transfer to the surface-bound species. In order to obtain the observed hydrocarbons, metastable reduced carbonate species should remain on the surface of CdS in near proximity to deposited copper islands in order to undergo multiple electron transfers.

Effect of Catalyst Configuration and Role of Na. In order to develop a plausible reaction mechanism for multiple electron transfer to CO_2 on functionalized CdS in light of the observed array of hydrocarbons, several points need to be addressed. First, the presence of Cu deposits on CdS appears to be essential for the formation of the C2 and C3 hydrocarbons. In the absence of Cu deposits (i.e., carried out as a control experiment), the remaining components (i.e., CdS-TNTs) alone did not produce C2 or C3 hydrocarbons under visible light irradiation. Cu complexes have been shown to be effective for the reduction of CO_2 into C1 and C2 hydrocarbons either photocatalytically or electrochemically.[1,12] However, in the present study, Cu was present on the surface as a metallic deposit, which remained unaltered after 5 h of photolysis in the presence of CO_2 (Figure S4, Supporting Information). The observed binding energy of Cu (Cu $2p_{3/2}$ at ∼933.5 eV) deposited on the CdS-TNTs matrix was higher than that usually observed for pure elemental Cu (Cu $2p_{3/2}$ at ∼932.6 eV). This is likely due to the effective back-donation of electrons from Cu to neighboring oxygen atoms of the supporting matrix and/or the cluster size effect[35−37] (i.e., blue shift of the binding energy with respect to the bulk metal including Au and Cu).

Second, the molecular configuration of the ternary hybrid catalyst appears to be critical.[38−40] For example, the observed hydrocarbon yields were higher in the case of CdS deposited onto Cu/TNTs (i.e., CdS/(Cu-TNTs)) by factors of 2−5 when compared to the case of Cu deposited onto CdS-TNTs (i.e., Cu/(CdS-TNTs)). This observation is consistent with the role of CdS in binding the CO_2 and the subsequent surface stabilization of the initial reduced species, $CO_2^{\bullet-}$.[41] Further evidence is provided by the DRIFT spectra, which show that surface-bound carbonate species form preferentially on CdS/(Cu-TNTs) over the Cu/(CdS-TNTs) composites (Figure S5, Supporting Information). This observation is also consistent with the data of Yang et al., who found no carbonate adsorbed on copper.[7] We had previously shown that ternary hybrid composites, which involved Pt metal deposits that were sandwiched between TiO_2 and CdS (i.e., CdS/(Pt-TiO_2)), were able to generate higher photocurrents compare to composite catalysts involving CdS sandwiched between Pt and TiO_2 (i.e., Pt/(CdS-TiO_2)).[25,40]

Last, the role of intercalated Na^+ within TNTs leading to increased CO_2 reduction needs to be addressed. Alkali metal dopants or additives have been established as being effective in enhancing CO_2 reduction at high temperatures due to the geometric and electronic effects induced in the core structure by the alkali metal ions.[34,42,43] This effect is clearly illustrated in Figure 3a, where increasing levels of Na^+ increased the measured rate of hydrocarbon production in a closed reaction system. The effect of alkali metal dopants is often attributed to a reduction in the work function of the catalyst.[44] The alkali-promoter effect appears to be more effective with respect to CO_2 photoreduction on the CdS/(Cu-TNTs) composite compared to that on the Cu/(CdS-TNTs) composite catalyst. This could be due to a higher probability for a close interaction between Cu and intercalated Na^+ near the surface of the underlying TNTs' support. The core TNT substrate may be considered to function as an electron-transfer promoter in addition to its role as a base-catalyst support.

In addition to promoting enhanced electron transfer to CO_2, the Na^+ promoter appears to have some impact on the formation of surface-bound carbonate, as illustrated in the DRIFT spectra of Figure 5. The peak intensities of the carbonate species appear to depend on the Na^+ level. In light of this effect, it has been noted previously that $CO_2^{\bullet-}$ is stabilized near alkali metal binding sites.[45] Additional evidence is provided by the XPS C 1s spectra (Figure S4, Supporting Information). The XPS spectra showed carbon appearing at a binding energy of 284.6 eV, while the broad peak at 287.6 eV was tentatively assigned to surface-bound carbonate species. The intensity of this peak was also a function of the intercalated fraction of Na^+ within $Na_xH_{2-x}Ti_3O_7$. The Na 1s spectrum of CdS/(Cu-TNTs) preloaded with CO_2 had two distinct peaks (Figure S1b, Supporting Information). The peak with a lower binding energy is characteristic of sodium oxide, while the peak at higher energy could be due to sodium, which arises from the reduction of Na^+ trapped inside of the carbon matrix.[46] These observations are consistent with the DRIFT spectra, which show that intercalated Na^+ within the $Na_xH_{2-x}Ti_3O_7$ core appears to favor the formation of surface-bound carbonate.

Reaction Mechanism. The photocatalytic reduction of CO_2 on CdS/(Cu-TNTs) is initiated most likely by a one-electron reduction to form $CO_2^{\bullet-}$, which in turns reacts with a H atom ($H^{\bullet}$) to produce hydrocarbons (Scheme 1). CO_2 hydrogenation leading to hydrocarbon formation appears to be a less likely pathway because of the absence of H_2 detected in the headspace of the photolysis reactor during 5 h of irradiation with visible light.

Transient radical formation was probed using DMPO as a spin trapping reagent followed by EPR characterization (Figure 6). However, clear signals of the DMPO−H or DMPO−CO_2 adducts were not found; on the other hand, signals for DMPO−CH_3 and DMPO−OH adducts were observed. The EPR signals were similar to those reported by Dimitrijevic et al.,

DOI: 10.1021/jp511329d
J. Phys. Chem. A 2015, 119, 4658−4666

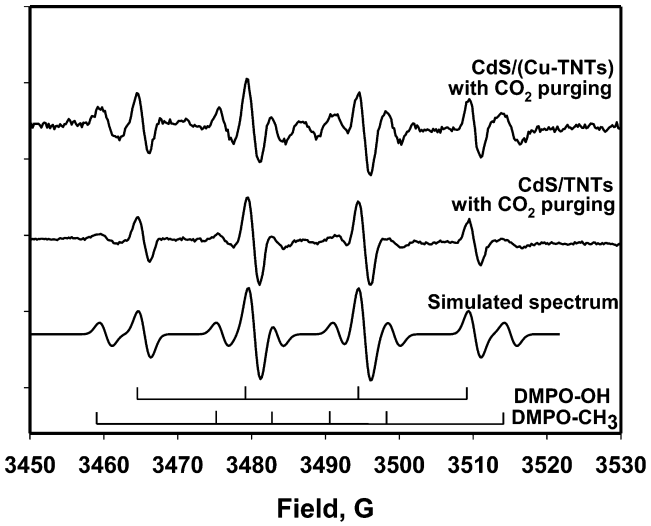

Figure 6. EPR spectra of DMPO−OH and DMPO−CH_3 adducts recorded at room temperature after 3 min of irradiation with visible light. No signals were observed for DMPO only.

who also noted an absence of DMPO−H and DMPO−CO_2 adducts during the photocatalytic reduction of CO_2 to CH_4, but they were able to observed signals for the methyl radical ($CH_3^{\bullet}$).[2] Even though the second-order rate constant for the self-reaction of the hydrogen atom in aqueous solution is high (R10; $k = 7.8 \times 10^9$ M^{-1} s^{-1}, while $k = 2.3 \times 10^{10}$ M^{-1} s^{-1} for R3),[47] the actual rate of R10 on a photocatalyst surface may be relatively slow compared to competitive pathways such as R4 (i.e., formate production).

Formate, which is formed near the Cu surface, may then undergo subsequent reductions by either trapped electrons or $H^{\bullet}$, yielding methyl radical and subsequently resulting in the observed products (R6−R9). However, $H^{\bullet}$ on the surface may react to reverse the above radical addition to re-form $CO_2^{\bullet-}$ (R5; $k = 1.91 \times 10^8$ M^{-1} s^{-1}).[47] If R5 takes place on the sodium trititanate nanotube surface, then the reaction sequence may proceed via the adsorbed carbonate species, and a sequence of successive photoinduced trapped electron reductions of the bound carbonate species is followed.

The absence of H_2 bubble formation is consistent with the lack of detectable DMPO−CO_2 and DMPO−H signals because the reaction of $H^{\bullet}$ with $CO_2^{\bullet-}$ (R4) on CdS/(Cu-TNTs) favors the formation of $CH_3^{\bullet}$ (R7). The hybrid combination involving Cu appears to be critical to the formation of $CH_3^{\bullet}$. This conclusion is consistent with the observation of low-intensity signals for DMPO−CH_3 on CdS-TNTs (Figure 6). Therefore, we assume that the formation $CH_3^{\bullet}$ is promoted either by direct electron transfer from the accumulated trapped electrons on Cu or by increasing the lifetimes of electron/hole pairs, leading to an increased probability of reaction. We also observed the formation of C1−C3 hydrocarbons when formate is used as a sacrificial electron donor under the same conditions. As we reported previously,[48] HCO_2^- could be catalytically oxidized to yield $CO_2^{\bullet-}$ and H^+, which are precursors leading to the formation of hydrocarbons on CdS/(Cu-TNTs) (Figure S6, Supporting Information) even in the presence of O_2 as a competitive electron acceptor.

CONCLUSIONS

This study showed that CdS/(Cu-TNTs) ternary composites can serve as catalysts for the photoreduction of CO_2 in the presence of water as an electron donor to form value-added C1−C3 hydrocarbons under visible light illumination. In this ternary configuration, photogenerated electrons are efficiently transported to elemental Cu through the titanate nanotube framework and effectively reduce CO_2 to C1−C3 hydrocarbons, while photogenerated holes oxidize water. Various spectrophotometric studies revealed that the one-electron reduced CO_2 ($CO_2^{\bullet-}$) reacts predominantly with multiple hydrogen atoms to form methyl radical ($CH_3^{\bullet}$). The absence of a H_2 bubble supports this reaction favored over the self-reactions of hydrogen atoms. The feasibility of utilizing simple inorganic photocatalytic systems for the reduction of CO_2 into useful hydrocarbons will depend, in part, on the stability and functionality of the catalyst. Although CdS undergoes photocorrosion in pure water, this hybrid composite appears to be stable in the presence of some electron donors that need to be treated.

ASSOCIATED CONTENT

Supporting Information

Figures S1−S6, including the O1s and Na1s spectra of CdS/(Cu-TNTs), effects of electron donors on time-profiled hydrocarbon formations on CdS/(Cu-TNTs), GC-MS spectra of methane, XPS Cu 2p spectra, Comparison of FTIR spectra between CO_2-preloaded CdS/(Cu-TNTs) and Cu/(CdS-TNTs), and Photocatalytic conversion of formic acid into C1−C4 hydrocarbons on CdS/(Cu-TNTs) as a function of O_2/N_2 ratio. This material is available free of charge via the Internet at http://pubs.acs.org.

AUTHOR INFORMATION

Corresponding Author

*E-mail: mrh@caltech.edu. Tel: 626-395-4391.

Notes

The authors declare no competing financial interest.

ACKNOWLEDGMENTS

Research support was funded by a National Science Foundation grant awarded to M.R.H. (Grant No. CHE-0924597). We acknowledge Dr. Nathan Dalleska for helping gas composition analysis at the Environmental Analysis Center, Environmental Science and Technology of California Institute of Technology (Caltech). We also acknowledge the technical staffs for the assistance of EPR and XRD works in the Division of Chemistry and Chemical engineering of Caltech. XPS and DRIFT experiments were carried out at the Molecular Materials Research Center of the Beckman Institute of Caltech. H.P. is grateful to the Korea National Research Foundation (2013K2A1A2052901, 2014S1A2A2027802, and 2014M1A3A3A02034875), the Korea Center for Artificial Photosynthesis (KCAP) (No. 2009-0093880), and the Korea CCS R&D Center (KCRC) (No. 2014M1A8A1049354) for financial support, and the Seoul Broadcasting System (SBS) Foundation in support of his sabbatical leave at Caltech.

REFERENCES

(1) Hoffmann, M. R.; Moss, J. A.; Baum, M. M. Artificial Photosynthesis: Semiconductor Photocatalytic Fixation of CO_2 to

DOI: 10.1021/jp511329d
J. Phys. Chem. A 2015, 119, 4658−4666

Afford Higher Organic Compounds. *Dalton Trans.* **2011**, *40*, 5151−5158.
(2) Dimitrijevic, N. M.; Vijayan, B. K.; Poluektov, O. G.; Rajh, T.; Gray, K. A.; He, H. Y.; Zapol, P. Role of Water and Carbonates in Photocatalytic Transformation of CO_2 to CH_4 on Titania. *J. Am. Chem. Soc.* **2011**, *133*, 3964−3971.
(3) Fujiwara, H.; Hosokawa, H.; Murakoshi, K.; Wada, Y.; Yanagida, S.; Okada, T.; Kobayashi, H. Effect of Surface Structures on Photocatalytic CO_2 Reduction Using Quantized CdS Nanocrystallites. *J. Phys. Chem. B* **1997**, *101*, 8270−8278.
(4) Indrakanti, V. P.; Kubicki, J. D.; Schobert, H. H. Photoinduced Activation of CO_2 on Ti-Based Heterogeneous Catalysts: Current State, Chemical Physics-Based Insights and Outlook. *Energy Environ. Sci.* **2009**, *2*, 745−758.
(5) Mikkelsen, M.; Jorgensen, M.; Krebs, F. C. The Teraton Challenge. A Review of Fixation and Transformation of Carbon Dioxide. *Energy Environ. Sci.* **2010**, *3*, 43−81.
(6) Olah, G. A.; Prakash, G. K. S.; Goeppert, A. Anthropogenic Chemical Carbon Cycle for a Sustainable Future. *J. Am. Chem. Soc.* **2011**, *133*, 12881−12898.
(7) Yang, C. C.; Yu, Y. H.; van der Linden, B.; Wu, J. C. S.; Mul, G. Artificial Photosynthesis over Crystalline TiO_2-Based Catalysts: Fact or Fiction? *J. Am. Chem. Soc.* **2010**, *132*, 8398−8406.
(8) Kim, W.; Seok, T.; Choi, W. Nafion Layer-Enhanced Photosynthetic Conversion of CO_2 into Hydrocarbons on TiO_2 Nanoparticles. *Energy Environ. Sci.* **2012**, *5*, 6066−6070.
(9) Kim, W.; Yuan, G.; McClure, B. A.; Frei, H. Light Induced Carbon Dioxide Reduction by Water at Binuclear $ZrOCo^{II}$ Unit Coupled to IR Oxide Nanocluster Catalyst. *J. Am. Chem. Soc.* **2014**, *136*, 11034−11042.
(10) Choi, S. K.; Kang, U.; Lee, S.; Ham, D. J.; Ji, S. M.; Park, H. Sn-Coupled p-Si Nanowire Arrays for Solar Formate Production from CO_2. *Adv. Energy Mater.* **2014**, *4*, 1301614.
(11) Hori, Y.; Murata, A.; Takahashi, R. Formation of Hydrocarbons in the Electrochemical Reduction of Carbon Dioxide at a Copper Electrode in Aqueous Solution. *J. Chem. Soc., Faraday Trans. 1* **1989**, *85*, 2309−2326.
(12) Peterson, A. A.; Abild-Pedersen, F.; Studt, F.; Rossmeisl, J.; Norskov, J. K. How Copper Catalyzes the Electroreduction of Carbon Dioxide into Hydrocarbon Fuels. *Energy Environ. Sci.* **2010**, *3*, 1311−1315.
(13) Kuhl, K. P.; Cave, E. R.; Abram, D. N.; Jaramillo, T. F. New Insights into the Electrochemical Reduction of Carbon Dioxide on Metallic Copper Surfaces. *Energy Environ. Sci.* **2012**, *5*, 7050−7059.
(14) Zhou, R.; Guzman, M. I. CO_2 Reduction under Periodic Illumination of ZnS. *J. Phys. Chem. C* **2014**, *118*, 11649−11656.
(15) Sekizawa, K.; Maeda, K.; Domen, K.; Koike, K.; Ishitani, O. Artificial Z-Scheme Constructed with a Supramolecular Metal Complex and Semiconductor for the Photocatalytic Reduction of CO_2. *J. Am. Chem. Soc.* **2013**, *135*, 4596−4599.
(16) Arai, T.; Sato, S.; Kajino, T.; Morikawa, T. Solar CO_2 Reduction Using H_2O by a Semiconductor/Metal-Complex Hybrid Photocatalyst: Enhanced Efficiency and Demonstration of a Wireless System Using $SrTiO_3$ Photoanodes. *Energy Environ. Sci.* **2013**, *6*, 1274−1282.
(17) Yadav, R. K.; Baeg, J.-O.; Oh, G. H.; Park, N.-J.; Kong, K.-j.; Kim, J.; Hwang, D. W.; Biswas, S. K. A Photocatalyst−Enzyme Coupled Artificial Photosynthesis System for Solar Energy in Production of Formic Acid from CO_2. *J. Am. Chem. Soc.* **2012**, *134*, 11455−11461.
(18) Tsai, C. W.; Chen, H. M.; Liu, R. S.; Asakura, K.; Chan, T. S. Ni@NiO Core−Shell Structure-Modified Nitrogen-Doped $InTaO_4$ for Solar-Driven Highly Efficient CO_2 Reduction to Methanol. *J. Phys. Chem. C* **2011**, *115*, 10180−10186.
(19) Varghese, O. K.; Paulose, M.; LaTempa, T. J.; Grimes, C. A. High-Rate Solar Photocatalytic Conversion of CO_2 and Water Vapor to Hydrocarbon Fuels. *Nano Lett.* **2009**, *9*, 731−737.
(20) Eggins, B. R.; Robertson, P. K. J.; Murphy, E. P.; Woods, E.; Irvine, J. T. S. Factors Affecting the Photoelectrochemical Fixation of Carbon Dioxide with Semiconductor Colloids. *J. Photochem. Photobiol., A* **1998**, *118*, 31−40.
(21) Sayama, K.; Arakawa, H. Photocatalytic Decomposition of Water and Photocatalytic Reduction of Carbon Dioxide Over ZrO_2 Catalyst. *J. Phys. Chem.* **1993**, *97*, 531−533.
(22) Chen, Q.; Zhou, Q.; Du, G.; Peng, L.-M. Trititanate Nanotubes Made via a Single Alkali Treatment. *Adv. Mater.* **2002**, *14*, 1208−1211.
(23) Du, G. H.; Chen, Q.; Che, R. C.; Yuan, Z. Y.; Peng, L.-M. Preparation and Structure Analysis of Titanium Oxide Nanotubes. *Appl. Phys. Lett.* **2001**, *79*, 3702.
(24) Kasuga, T.; Hiramatsu, M.; Hoson, A.; Sekino, T.; Niihara, K. Titania Nanotubes Prepared by Chemical Processing. *Adv. Mater.* **1999**, *11*, 1307−1311.
(25) Park, H.; Choi, W.; Hoffmann, M. R. Effects of the Preparation Method of the Ternary $CdS/TiO_2/Pt$ Hybrid Photocatalysts on Visible Light-Induced Hydrogen Production. *J. Mater. Chem.* **2008**, *18*, 2379−2385.
(26) Kim, Y. K.; Park, H. Light-Harvesting Multi-Walled Carbon Nanotubes and CdS Hybrids: Application to Photocatalytic Hydrogen Production from Water. *Energy Environ. Sci.* **2011**, *4*, 685−694.
(27) Silva, L. A.; Ryu, S. Y.; Choi, J.; Choi, W.; Hoffmann, M. R. Photocatalytic Hydrogen Production with Visible Light over Pt-Interlinked Hybrid Composites of Cubic-Phase and Hexagonal-Phase CdS. *J. Phys. Chem. C* **2008**, *112*, 12069−12073.
(28) Mekki, A.; Holland, D.; McConville, C. F. X-ray Photoelectron Spectroscopy Study of Copper Sodium Silicate Glass Surfaces. *J. Non-Cryst. Solids* **1997**, *215*, 271−282.
(29) Takeda, H.; Koike, K.; Inoue, H.; Ishitani, O. Development of an Efficient Photocatalytic System for CO_2 Reduction Using Rhenium(l) Complexes Based on Mechanistic Studies. *J. Am. Chem. Soc.* **2008**, *130*, 2023−2031.
(30) Morgenstern, D. A.; Wittrig, R. E.; Fanwick, P. E.; Kubiak, C. P. Photoreduction of Carbon Dioxde to Its Radical Anion by $[Ni_3(\mu_3\text{-}I)_2(dppm)_3]$: Formation of Two Carbon−Carbon Bonds via Addition of CO_2^- to Cyclohexene. *J. Am. Chem. Soc.* **1993**, *115*, 6470−6471.
(31) Choi, S. K.; Kim, S.; Lim, S. K.; Park, H. Photocatalytic Comparison of TiO_2 Nanoparticles and Electrospun TiO_2 Nanofibers: Effects of Mesoporosity and Interparticle Charge Transfer. *J. Phys. Chem. C* **2010**, *114*, 16475−16480.
(32) Khan, G.; Kim, Y. K.; Choi, S. K.; Han, D. S.; Abdel-Wahab, A.; Park, H. Evaluating the Catalytic Effects of Carbon Materials on the Photocatalytic Reduction and Oxidation Reactions of TiO_2. *Bull. Korean Chem. Soc.* **2013**, *34*, 1137−1144.
(33) Kim, Y. K.; Khan, G.; Jeong, H. W.; Park, H. SWNTs-Catalyzed Solar Hydrogen Production. *Rapid Commun. Photosci.* **2014**, *3*, 56−58.
(34) Du, H.; Williams, C. T.; Ebner, A. D.; Ritter, J. A. In Situ FTIR Spectroscopic Analysis of Carbonate Transformations during Adsorption and Desorption of CO_2 in K-Promoted HTlc. *Chem. Mater.* **2010**, *22*, 3519−3526.
(35) Ferretti, N.; Balkaya, B.; Volmmer, A.; Neeb, M.; Eberhardt, W. Inner-Shell Photoelectron Spectroscopy of Size-Selected Cu-Clusters on Si. *J. Electron Spectroscopy.* **2007**, *156−158*, 124−127.
(36) Gadzuk, J. W.; Sunjic, M. Excitation Energy Dependence of Core-Levle X-ray-Photoemission-Spectra Line Shapes in Metals. *Phys. Rev. B* **1975**, *12*, 524−530.
(37) Peters, S.; Peredkov, S.; Neeb, M.; Eberhardt, W.; Al-Hada, M. Size-Dependent XPS Spectra of Samll Supported Au-Clusters. *Surf. Sci.* **2013**, *608*, 129−134.
(38) Jang, J. S.; Park, H. Strategic Design of Heterojunction CdS Photocatalysts for Solar Hydrogen. In *Materials and Processes for Solar Fuel Production*; Viswanathan, B., Subramanian, V., Lee, J. S., Eds.; Springer: Berlin, Germany, 2014.
(39) Khan, G.; Choi, S. K.; Kim, S.; Lim, S. K.; Jang, J. S.; Park, H. Carbon Nanotubes as an Auxiliary Catalyst in Heterojunction Photocatalysis for Solar Hydrogen. *Appl. Catal., B* **2013**, *142*, 647−653.
(40) Park, H.; Kim, Y. K.; Choi, W. Reversing CdS Preparation Order and Its Effects on Photocatalytic Hydrogen Production of CdS/

DOI: 10.1021/jp511329d
J. Phys. Chem. A 2015, 119, 4658−4666

Pt-TiO_2 Hybrids under Visible Light. *J. Phys. Chem. C* **2011**, *115*, 6141−6148.
(41) Fujiwara, H.; Kanemoto, M.; Ankyu, H.; Murakoshi, K.; Wada, Y.; Yanagida, S. Visible-Light Induced Photofixation of Carbon Dioxide into Aromatic Ketones and Benzyl Halides Catalysed by CdS Nanocrystallites. *J. Chem. Soc., Perkin Trans. 2* **1997**, 317−321.
(42) Panagiotopoulou, P.; Kondarides, D. I. Effects of Alkali Promotion of TiO_2 on the Chemisorptive Properties and Water−Gas Shift Activity of Supported Noble Metal Catalysts. *J. Catal.* **2009**, *267*, 57−66.
(43) Vayenas, C. G.; Bebelis, S.; Pliangos, C.; Brosda, S.; Tsiplakides, D. *Electrochemical Activation of Catalysis*; Springer: New York, 2001.
(44) Holzl, J.; Schulte, F. K. Work Function of Metals. *Solid Surf. Phys.* **1979**, *85*, 1−150.
(45) Kiskinove, M. P. *Poisoning and Promotion in Catalysis based on Surface Science Concepts and Experiments*; Elsevier: The Netherlands, 1992.
(46) Lukaszewicz, J. P.; Panas, M.; Siedlewski, J. Sodium-Doped Carbon Films for Humidity Sensor Construction. *Sens. Actuator, B* **1996**, *32*, 221−226.
(47) Buxton, G. V.; Greenstock, C. L.; Helman, P.; Ross, A. B. Critical Review of Rate Constants for Reactions of Hydrated Electrons, Hydrogen Atoms and Hydroxyl Radicals in Aqueous Solution. *J. Phys. Chem. Ref. Data* **1988**, *17*, 513−886.
(48) Mrowetz, M.; Balcerski, W.; Colussi, A. J.; Hoffmann, M. R. Oxidative Power of Nitrogen-Doped TiO_2 Photocatalysts under Visible Illumination. *J. Phys. Chem. B* **2004**, *108*, 17269−17273.

DOI: 10.1021/jp511329d
J. Phys. Chem. A 2015, 119, 4658−4666